Journal of Catalysis **200,** 321–329 (2001)
doi:10.1006/jcat.2001.3211, available online at http://www.idealibrary.com on IDEAL®

In Situ EXAFS Study of Rh/Al_2O_3 Catalysts for Catalytic Partial Oxidation of Methane

Jan-Dierk Grunwaldt,*,[1] Luca Basini,† and Bjerne S. Clausen*

*Haldor Topsøe A/S, Nymøllevej 55, DK-2800 Lyngby, Denmark; and †Snamprogetti S.p.A., Via Maritano 26, 20097, San Donato Milanese, Milan, Italy

Received November 16, 2000; revised February 22, 2001; accepted February 22, 2001; published online May 16, 2001

Alumina-supported rhodium particles, active for the catalytic partial oxidation (CPO) of methane, have been investigated by *in situ* X-ray absorption fine structure (XAFS), monitoring the gas composition simultaneously by mass spectrometry. The catalysts were prepared by anchoring of $Rh_4(CO)_{12}$ onto the support and activated by treatments in He and H_2. EXAFS analyses showed that the Rh carbonyl precursor maintained its structure during fixation, but decomposed to small metallic Rh particles upon heating in He. However, the particle size increased significantly during treatment in hydrogen. Investigations of the catalyst in the CH_4/O_2 reaction mixture showed that the CPO reaction ignited at about 330°C and, at the same time, the catalyst changed its structure. The metal particles disaggregated upon heating in the reaction mixture and some Rh clusters containing oxidic or carbonylic species were formed. This process was reversible with respect to temperature. The selectivity of the catalyst in the CH_4/O_2 reaction mixture was significantly dependent on the residence time. However, no significant structural differences of the Rh particles have been found at different residence times. Additionally, catalyst oxidation and reduction were investigated upon O_2 and CH_4 treatment.

1. INTRODUCTION

Gas-to-liquid (GTL) technologies are attracting increasing attention with respect to conversion of natural gas into liquid products such as methanol, DME, or synthetic fuels. The first step is the production of synthesis gas, i.e., a mixture of hydrogen and carbon oxides. Well-established and commercial technologies include tubular steam reforming, autothermal reforming, or combinations thereof (1–4). The optimal choice depends on the desired final product and the plant capacity (4).

A potential new technology studied extensively is catalytic partial oxidation of natural gas (shown below for methane):

$$CH_4 + \tfrac{1}{2}O_2 \rightarrow CO + 2H_2 \quad \Delta H_{298K} = -38 \text{ kJ/mol}.$$

[1] To whom correspondence should be addressed. E-mail: jdg@topsoe.dk.

Catalytic partial oxidation is not a new idea. Work on nickel catalysts has already been subject to many studies since 1946 (5–7). Presently, many promising catalytic systems are known, among them Co, Ni, and especially noble metals on different supports (cf. (8–10)). While most of the work before 1992 considered reaction conditions with residence times (τ) above 0.1 s, the CPO reaction attracted especially new interest when it was reported that high yields of CO could be obtained even at residence times of 10^{-3} s or below (11–17). High yields of CO have, e.g., been reported on Ir, Rh, Pd, and Pt clusters (18–20). Among them, Rh on MgO, Al_2O_3, and CeO_2 is of interest because it has high resistance against carbon formation (9, 21, 22). The selectivity dependence of the reaction on the residence time has been studied in detail, showing that significant changes are found at $\tau < 0.1$ s (21–24). However, no final agreement on the reaction mechanism has been obtained and the surface and bulk structures of the metal particles are difficult to determine under reaction conditions.

The aim of this study is to obtain more insight into the particle structure of Rh clusters under reaction conditions. While diffuse reflectance infrared Fourier transform spectroscopy (DRIFTS) studies have recently been performed under CPO reaction conditions (21) to study the structure of the reacting clusters, EXAFS can give complementary information on the bulk structure of the Rh particles. Extended X-ray absorption fine structure spectroscopy (EXAFS) has been used in several studies to obtain information on the structure (oxidation state, identity of neighbouring atoms, and particle size) of Rh catalysts (25–31) but not during catalysis. Since the structure of the Rh particles is strongly dependent on the gaseous atmosphere applied (e.g., restructuring occurs when exposing the Rh surface with CO or O_2 instead of H_2 (25, 26, 30, 32, 33)), *in situ* studies are inevitable for studying the physico-chemical structure of these Rh clusters. However, none of the *in situ* XAFS studies have been performed under CPO reaction conditions. Hence, we applied the XAFS technique to study *in situ* the Rh/Al_2O_3 catalyst during activation and under CPO reaction conditions. Simultaneous to the EXAFS

0021-9517/01 $35.00

measurements, on-line product analysis by mass spectrometry was performed to obtain a relationship between the catalytic activity and the structure of the clusters. For this purpose a capillary microreactor was used (34–36), which is ideal both for structural characterization and for on-line catalytic studies at relatively short residence times.

In situ XAFS studies have been performed during the decomposition of the carbonyl precursor, the formation of the metallic rhodium particles, and the catalytic reaction using two different residence times. For comparison also some *in situ* XRD measurements have been carried out. Additionally, gas treatments in oxidizing (O_2 in He) and reducing (CH_4 in Ar) atmospheres were carried out to draw further conclusions on the structure of the catalyst under CPO reaction conditions. To compare with previous results, the reaction sequences were similar to those investigated previously by DRIFTS (18, 20–22), and the catalysts were prepared in the same way by fixation of a $Rh_4(CO)_{12}$ precursor on the Al_2O_3 support.

2. EXPERIMENTAL

Preparation. The catalysts used in this study were prepared by the same procedure as described in Refs. (21, 37). It consisted of the preparation of a $Rh_4(CO)_{12}$ precursor (38) and a slurry of α-Al_2O_3 (Aldrich 99.999%, dispersed in hexane). The precursor was anchored on the alumina support through a solid–liquid reaction in hexane in a CO atmosphere. For EXAFS studies catalysts with 5 wt% Rh loading were used.

Reaction cell. For both EXAFS and XRD studies the reaction cell consisted of a quartz capillary tube (wall thickness $d = 0.02$ mm, outer diameter $\phi = 0.7$ mm) in which the catalyst ($\approx$10 mg, sieved fraction 75–125 μm) was loaded between two pieces of glass wool. The sample was heated (and cooled) by passing a hot (or cold) N_2 gas stream, whose temperature was regulated by a Eurotherm controller, over the capillary tube. Temperature homogeneity was ensured by enclosing the reactor in an X-ray transparent heat shield. The temperature was monitored by a thermocouple directly beneath the sample. The capillary tube was connected via stainless steel tubes to a gas system with different premixed gases and mass flow controllers. Further details on the *in situ* setup are described in Refs. (35, 39, 40).

The gas composition was monitored by a mass spectrometer (Balzers Thermostar) after the gas was passed over the catalyst. The gas flow was normally held constant to 5 ml/min, except for the CH_4/O_2 reaction mixture, where the flow was varied between 1 and 12 ml/min, resulting in residence times around 0.54 and 0.045 s. The following gas mixtures were used: (1) pure He; (2) 2% O_2 in He; (3) 10% CH_4 in Ar; (4) 6% $CH_4 + 3\%$ O_2 in He; (5) 2% H_2 in N_2. The following experiments, which were analogous to the DRIFTS experiments in Refs. (18, 20–22), were performed:

TABLE 1

Overview on the Performed Experiments and Experimental Details (in All Experiments the Temperature Ramp Was 5°C/min)

Step	Gas mixture	Reaction temperature (°C)	Flow (ml/min)	Residence time τ(s)
A	He	500	5	0.11
B	2% H_2 in N_2	500	5	0.11
C	6% CH_4 + 3% O_2	600	1 and 12	0.54 and 0.045
D	2% O_2 in He	500	5	0.11
E	10% CH_4 in Ar	500	5	0.11

(A) decomposition of the precursor in He; (B) reduction in H_2; (C) reaction in the CH_4/O_2 mixture; (D) oxidation of catalyst after step A in O_2; (E) reduction of the oxidized catalyst in CH_4 (after step D).

The temperature ramp and the target temperatures are listed in Table 1. In general, the normal EXAFS spectra were taken at RT before the experiment was started, at the reaction temperatures, and after quenching the catalyst in the corresponding reaction mixture to room temperature. The transient behaviour was recorded by quick EXAFS (QEXAFS) scans.

EXAFS setup and analysis. EXAFS spectra were measured in the transmission geometry at HASYLAB, DESY (Hamburg, Germany), at the RÖMO II experimental station at beam X1. Two parallel Si(311) crystals were used for monochromatization of the X-rays. Higher harmonics were minimized by slightly detuning the crystals. Three ionization chambers filled with Ar gas were used to record the intensity of the incident and transmitted X-rays. The *in situ* cell was located between the first and the second ionization chamber, and a Rh foil (edge energy at 23,219.8 eV) between the second and the third ionization chamber was used as a reference sample for accurate energy calibration of the EXAFS spectra.

XAFS spectra were recorded around the K-edge of Rh (23,219.8 keV) between 22,900 and 24,200 eV by step scanning the monochromator. Additionally, QEXAFS data (40) were collected *in situ* during reaction and heating in the region 23,000–23,800 eV by moving the monochromator at a constant angular speed (120–130 s/spectrum).

Standard data analyses including deglitching, pre-edge subtraction, background subtraction, normalization, and Fourier transformation were performed. For the spectra shown here, Fourier transformation was applied on the k^1-weighted and k^3-weighted $\chi(k)$ functions in the interval $k = 2.5$–15.5 Å^{-1}. The peak in the Fourier transformation was filtered and then inversely Fourier-transformed back into k-space. The backscattering amplitudes and phase shifts of the nearest neighbour Rh–Rh and Rh–O contributions were taken from model samples (Rh foil and Rh_2O_3), assuming for the first shell of Rh metal a

coordination number of 12 and a Rh–Rh distance of 2.68 Å and for the first shell of Rh_2O_3 an oxygen coordination number of 6 and a Rh–O distance of 2.05 Å. Additionally, room-temperature EXAFS spectra were recorded of the model sample, $Rh_4(CO)_{12}$.

3. RESULTS AND DISCUSSION

3.1. Analysis of the As-Prepared Catalyst

Figure 1 shows the Fourier-transformed EXAFS spectrum of the catalyst obtained after anchoring the Rh-carbonyl complex on the alumina support. Moreover, the Fourier-transformed spectra of the model compounds, Rh metal, Rh_2O_3, and the pure $Rh_4(CO)_{12}$ complex, which were used in the preparation process, are depicted. Note that the distance scale in the Fourier-transformed spectra is not corrected for the phase shift. The Fourier-transformed EXAFS spectra at the Rh K-edge of the fresh catalyst and the Rh-carbonyl precursor are very similar and two peaks are visible. One peak with large contribution is located around 1.5 Å and a smaller peak at about 2.5 Å. Comparison with the model samples reveals that the first peak in the spectrum probably corresponds to the Rh–O or the Rh–C shell (first shell), whereas the second is due to the Rh–Rh shell (second shell). To obtain more quantitative data, the peak at 2.5 Å was fitted using backscattering amplitudes and phase shifts for the Rh–Rh shell from the Rh foil. Additionally, the first shell (here mainly Rh–C) was fitted with the help of data extracted from the pure metal carbonyl complex $Rh_4(CO)_{12}$ ($r_{Rh-C} = 1.97$ Å; $r_{Rh-Rh} = 2.73$ Å, Ref. (38)).

Table 2 (k^1-weighted EXAFS function) and Table 3 (k^3-weighted) give the results for the fitted Rh–Rh distances, R_2, and the number of nearest neighbours, N_2. Additionally, the vibrational amplitude σ and the energy shift ΔE are given (41). The distance and coordination number of the fresh catalyst before treatment are quite similar to the $Rh_4(CO)_{12}$ precursor, showing that the local structure of the rhodium carbonyl cluster is partly retained during deposition. The Rh–Rh distance in the metal carbonyl cluster is slightly lower than that in the $Rh_4(CO)_{12}$ cluster and very close to that of the Rh–Rh foil, and the coordination number of the fresh catalyst is around 3, as expected from the crystal structure of the carbonyl compound (38). The coordination number from k^3-weighted functions was lower than 3, which may be due to anharmonic effects (cf. (42)).

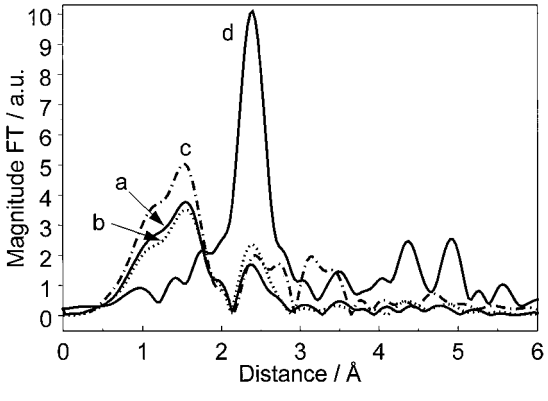

FIG. 1. Fourier transform of the Rh K-edge EXAFS spectra (k^1-weighted) of (a) freshly prepared Rh/Al_2O_3, (b) $Rh_4(CO)_{12}$, (c) Rh_2O_3, and (d) Rh foil.

Table 4 shows the fitting results for the first shell of the Rh/Al_2O_3 catalyst. The coordination number for the fresh catalyst is slightly increased compared to that of the pure compound. Since a typical Rh–O distance (e.g., in Rh_2O_3) is around 2.05 Å and the Rh–C distance in the carbonyl clusters is around 2.0 Å (1.97 Å in the case of $Rh_4(CO)_{12}$), the Rh–C and Rh–O shell cannot be easily distinguished. The low Rh–Rh coordination number (Tables 2 and 3) for the untreated catalyst and the slightly increased coordination number of the Rh–C/Rh–O shell (Table 4) exclude the formation of higher coordinated Rh carbonyl clusters (e.g., $Rh_6(CO)_{16}$). The results can be explained with additional Rh–O interactions or distortions, resulting e.g. from the interaction between the Rh clusters and the Al_2O_3 support. DRIFTS studies have shown (37) that a $Rh^I(CO)_2$ species forms through reductive disaggregation when using 0.1% Rh loading. Although the EXAFS analysis indicates that the $Rh_4(CO)_{12}$ complex is retained during the deposition process, $Rh^I(CO)_2$ may also be formed in the present catalysts with a higher metal loading. However, EXAFS is not sensitive enough to uncover this species because the EXAFS signals refer to an average situation.

3.2. Step A (Heating in He)

Figure 2 depicts the development of the QEXAFS spectra at the near edge region of the Rh K-edge upon heating in an inert He atmosphere. The structure of the sample starts changing above ~170°C as indicated by the decrease of the whiteline (intense feature at 23,230 eV in Fig. 2) and the formation of a second peak at 23,250 eV. This reveals that the carbonyl complex gradually decomposes and metallic particles form as also evidenced by stronger oscillations above 23,320 eV. In parallel, some CO and CO_2 release is detected by mass spectrometer analyses during heating due to the decomposition of the complex. Figure 3 shows a comparison of the Fourier transform of the EXAFS spectrum (recorded at room temperature) after heating of the catalyst to 500°C in He and that of the untreated catalyst (compare graphs a and b). The contribution of the Rh–Rh shell increases significantly compared to the fresh catalyst. Since the apparent coordination number CN = 7.0 of the Rh–Rh shell (Tables 2 and 3) is significantly smaller than that of the Rh metal, small metallic Rh particles seem to form upon this treatment. According to Fig. 3b there is a small contribution of the first shell around 1.7 Å. The analysis (Table 4)

TABLE 2

EXAFS Parameters (Coordination Number, N_2, and Rh–Rh Distance, R_2) of RT Spectra after the Different Reaction Steps (Fit of the Second Shell (Rh–Rh Shell), k^1-Weighted Functions, Backscattering Amplitudes, and Phase Shifts Taken from the Rh Foil as Reference, Backtransform between 2.0 and 3.2 Å)

Catalyst	Conditions	N_2	R_2 (Å)	σ (Å)	ΔE (eV)	χ^{2a}
Rh/Al_2O_3	Before treatment	3.0 ± 0.5	2.67 ± 0.02	0.10	−1.3	0.042
Rh/Al_2O_3	After heating in He (step A)	7.1 ± 0.5	2.69 ± 0.02	0.09	−2.6	0.0040
Rh/Al_2O_3	After heating in H_2 (step B)	11.2 ± 0.5	2.69 ± 0.02	0.09	−1.4	0.0011
Rh/Al_2O_3	After heating in CH_4/O_2 (step C)	10.1 ± 0.5	2.69 ± 0.02	0.09	−1.8	0.0023
Rh/Al_2O_3	After heating in O_2 (step D)	—	—	—	—	No fit possible
Rh/Al_2O_3	After heating in CH_4 (step E)	12.2 ± 0.5	2.71 ± 0.02	0.09	−1.7	0.0040

[a] Fitting accuracy, defined as $\chi^2 = \Sigma(\chi_{obs} - \chi_{cal})^2/\Sigma\chi^2_{obs}$.

shows that scattering from Rh–C or Rh–O only contributes slightly and therefore it can be concluded that only small amounts of e.g. carbidic, oxidic, or carbonylic species remained in the Rh clusters. Due to the low contribution to the first shell, the fitting accuracy χ^2 is also relatively low. DRIFT spectra (37) revealed that all CO stretching bands disappear at temperatures higher than 300°C on Rh/Al_2O_3, which is in agreement with the EXAFS data, and carbonylic species are obviously removed.

3.3. Step B (Reduction in H_2)

Upon reduction to 500°C in H_2, the catalyst is further reduced as evidenced by *in situ* QEXAFS (decrease of white-line) and by more pronounced EXAFS oscillations. The catalyst is almost fully reduced at 175°C. After reduction at 500°C, the metal particles seem to increase significantly as seen from the large contribution of the Rh–Rh shell (Fig. 3). The Fourier-transformed spectrum looks very similar to the reference spectrum of a Rh foil. The increase of the particle size is also reflected by the high coordination number of Rh obtained by fitting of the Rh–Rh shell (Tables 2 and 3). Also, the fit of the third Rh–Rh shell ($R_{Rh-Rh} = 4.66$) resulted in a high coordination number (Table 5), indicating relatively large particles. *In situ* XRD studies on catalysts subjected to similar treatments showed that weak diffraction lines appeared at $2\Theta = 47°$ and $2\Theta = 41°$. The line at 41° partly overlapped with a line from the alumina support. From the line width at $2\Theta = 47°$, a crystallite size of about 60 Å using the Debye Scherrer formula can be estimated. This indicates that the particles are still quite small. Also, the investigation of the Rh/Al_2O_3 catalysts in the DRIFTS cell has shown that some remaining bands in the 1900- to 2050-cm^{-1} range disappeared above 300°C during this treatment in H_2 (37). Hence, the advantage of the Rh-carbonyl precursor is that it is easily decomposed, compared to e.g. a Rh–Cl based precursor (27), which still showed some Rh–Cl–contribution after reduction at 400°C.

3.4. Step C (Reaction Mixture)

In the third step the hydrogen-reduced Rh catalyst was investigated under reaction conditions in a $6\%CH_4/3\%O_2$/He gas mixture. The temperature-dependent mass spectra with selected MS signals are depicted in Figs. 4a (flow: 1 ml/min) and 4b (flow 12 ml/min). The CPO reaction with the formation of hydrogen and carbon monoxide ignited at 320–330°C, when using a flow of 1 ml/min (residence time 0.54 s). The signals for the products ($m/e = 28$ for CO and ($m/e = 2$ for H_2) sharply increased above these temperatures, while the signals for the reactants ($m/e = 15$ and $m/e = 16$ for methane, $m/e = 32$ for O_2) decreased. The consumption of methane and oxygen partly starts below the ignition temperature and different behaviours are observed for the methane consumption as a function of the temperature before and after the ignition of the CPO reaction

TABLE 3

EXAFS Parameters (Coordination Number, N_2, and Rh–Rh Distance, R_2) of RT Spectra after the Different Reaction Steps (Fit of the Second Shell (Rh–Rh Shell), k^3-Weighted Functions, Backscattering Amplitudes, and Phase Shifts Taken from the Rh Foil as Reference, Backtransform between 2.0 and 3.2 Å)

Catalyst	Conditions	N_2	R_2 (Å)	σ (Å)	ΔE (ev)	χ^2
Rh/Al_2O_3	Before treatment	2.0 ± 0.5	2.67 ± 0.02	0.09	1.3	0.010
Rh/Al_2O_3	After heating in He (step A)	6.9 ± 0.5	2.69 ± 0.02	0.09	−1.8	0.0006
Rh/Al_2O_3	After heating in H_2 (step B)	10.3 ± 0.5	2.69 ± 0.02	0.09	−1.7	0.0009
Rh/Al_2O_3	After heating in CH_4/O_2 (step C)	9.3 ± 0.5	2.69 ± 0.02	0.09	−1.3	0.0007
Rh/Al_2O_3	After heating in CH_4 (step E)	12.0 ± 0.5	2.68 ± 0.02	0.09	−1.1	0.0033

TABLE 4

EXAFS Parameters of RT Spectra after the Different Steps (Fit of the First Shell with Parameters from $Rh_4(CO)_{12}$ in BN, Backtransform between 0.4–2.0 Å, Coordination Number, N_1, and Rh–C/Rh–O Distance, R_1)

Catalyst	Conditions	N_1	R_1 (Å)	σ (Å)	ΔE (eV)	χ^2
Rh/Al_2O_3	Before treatment	3.2 ± 0.5	2.00 ± 0.02	0.086	−0.5	0.0029
Rh/Al_2O_3	After heating in He (step A)	2.0 ± 0.5	2.07 ± 0.05	0.10	−5.0	0.016
Rh/Al_2O_3	After heating in H_2 (step B)	1.5 ± 0.5	2.12 ± 0.05	0.10	−11	0.1[a]
Rh/Al_2O_3	After heating in CH_4/O_2 (step C)	1.5 ± 0.5	2.09 ± 0.05	0.10	−9.8	0.1[a]
Rh/Al_2O_3	After heating in O_2 (step D)	5.2 ± 0.5	2.04 ± 0.05	0.084	−0.1	0.0027

[a] Poor fit, as also indicated by fitting accuracy due to low contribution.

(Fig. 4). Above the ignition point, the remaining oxygen concentration in the outlet gas stream is very small. The formation of the by-products water ($m/e = 18$) and CO_2 ($m/e = 44$) is observed particularly at low temperatures, while the selectivity toward H_2 and CO increases above the ignition point. This is in agreement with previously reported results (22, 23). When a higher flow velocity is used (12 ml/min, residence time ca. 0.045 s), the reaction to hydrogen and carbon monoxide also ignites at about 330°C (Figure 4b). Methane and oxygen consumption together with H_2 and CO formation begin sharply around the ignition point. The maximum for CO_2 and H_2O formation is already reached at lower temperatures (compare Figs. 4a and 4b). Thus, the experiment shows some evidences concerning an apparently higher selectivity toward H_2 and CO when using shorter residence times.

The corresponding QEXAFS data, obtained *simultaneously* on the *same* sample, are shown in Fig. 5. We only depict the results for the first case with a flow of 1 ml/min. Essentially, the same behaviour was observed in EXAFS at higher flows. Between 50 and 300°C, the catalyst gradually changes its structure (Fig. 5(1)). The whiteline increases and the edge shifts slightly to higher energies, indicating that Rh is first slightly oxidized. Around 320°C, the structure of the catalyst is abruptly changed within less than 15°C (Fig. 5(2)), about the same temperature where the CPO reaction initiated (Fig. 4a). The whiteline significantly decreases, indicating that Rh is reduced again. A comparison of the room-temperature EXAFS spectra after reduction in H_2/N_2 (step B) and after the CH_4/O_2 reaction mixture revealed that apart from a slightly smaller peak intensity there is no significant difference (Fig. 6(1) and Tables 2 and 3). The analysis of the third Rh–Rh shell ($R_{Rh-Rh} = 4.66$ Å, Table 5) also indicates that the coordination number is slightly decreased. However, significant differences are found between the catalyst in a CH_4/O_2 atmosphere and in a H_2/N_2 atmosphere at high temperature as shown in Fig. 6(2).

The intensity of the peak in the Fourier transform located around 2.5 Å (Rh–Rh shell) is significantly lower in a CH_4/O_2 atmosphere than in a H_2/N_2 atmosphere, indicating smaller particles. This is also supported by the weak peaks at higher R values (Fig. 6(2), and e.g. the third Rh–Rh shell (Table 5)), which confirm that higher shells do not contribute to the EXAFS spectrum. While a relatively good fit of the third shell is obtained for the sample reduced at 500°C in H_2, the fit is relatively poor for the corresponding spectrum of the sample in the CH_4/O_2 mixture at 600°C. Thus, the rhodium metal particles are re-dispersed upon heating in the reaction mixture.

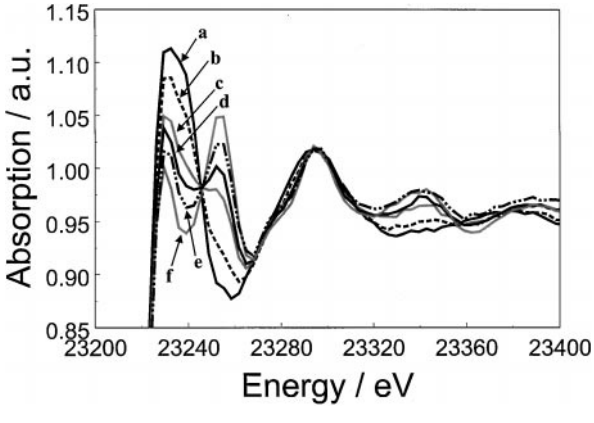

FIG. 2. *In situ* QEXAFS spectra of the Rh K-edge during heating in He (step A): (a) 100°C, (b) 170°C, (c) 210°C, (d) 275°C, (e) 350°C, and (f) 420°C.

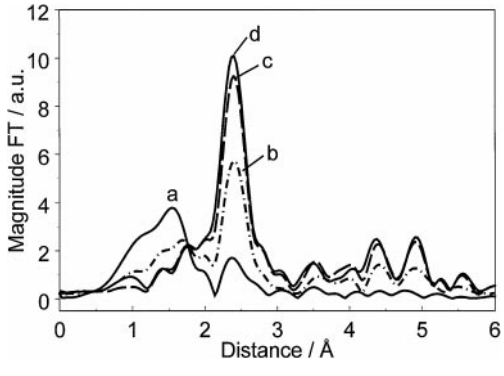

FIG. 3. Fourier transforms of *in situ* k^1-weighted EXAFS oscillations of a Rh/Al_2O_3 catalyst at room temperature: (a) fresh catalyst, (b) after treatment at 500°C in He (after step A), (c) at 500°C in H_2 (after step B), and (d) Rh foil.

TABLE 5

EXAFS Parameters (Coordination Number, N_3, and Rh–Rh Distance, R_3) of RT Spectra after Different Treatments (Fit of the Third Rh–Rh Shell, k^3-Weighted Functions, Backscattering Amplitudes, and Phase Shifts Taken from the Rh Foil as Reference, R_{Rh-Rh} = 4.66, Backtransform between 3.8 and 4.8 Å)

Catalyst	Conditions	N_3	R_3 (Å)	σ (Å)	ΔE (eV)	χ^2
Rh/Al_2O_3	Before treatment	—[a]	—[a]	—[a]	—[a]	—[a]
Rh/Al_2O_3	After heating in He (step A)	8.2 ± 0.5	4.70 ± 0.02	0.10	−4.5	0.023
Rh/Al_2O_3	After heating in H_2 (step B)	10.6 ± 0.5	4.69 ± 0.02	0.09	−3.0	0.0036
Rh/Al_2O_3	After heating in CH_4/O_2 (step C)	8.9 ± 0.5	4.68 ± 0.02	0.09	0.1	0.0027
Rh/Al_2O_3	After heating in H_2 (step B, at 500°C)	7.5 ± 0.5	4.69 ± 0.02	0.08	−8.0	0.0066
Rh/Al_2O_3	After heating in CH_4/O_2 (step C, at 600°C)	4.4 ± 0.5	4.68 ± 0.02	0.12	0.1	0.29^x

[a] Poor fit, as also indicated by fitting accuracy due to low contribution.

The process is reversible with respect to temperature, and slight oxidation up to 320°C and ignition of the reaction at 320–330°C accompanied by reduction of Rh and its re-dispersion can be observed in several cycles by a combined EXAFS/on-line gas analysis. EXAFS also shows that cooling in the reaction mixture changes the catalyst structure, leading to nearly the same catalyst state as before treatment C, i.e., large Rh particles. Although high-temperature short contact time CPO of methane has been performed in lab-scale reactors at temperatures higher than 1000°C, it seems that the results at 600°C are representative and the significant structural changes occur at the ignition temperature of the CPO reaction.

Although the catalysts during CPO reaction conditions are reduced (no whiteline), the small contribution in the Fourier-transformed spectra at $R = 1.7$ Å indicates that some carbonyl or oxygen species are present in the catalyst particles (see also Table 4). CO adsorption on the Rh catalysts, as reported in the literature (25, 26, 43), led to a strong decrease in the amplitude at $E > 23{,}320$ eV, probably due to the formation of Rh-carbonyls. Surface carbonyl clusters were also reported in a recent DRIFTS study (21, 22) where similar reaction conditions and similar catalysts as in the present study were used. In an EXAFS study, Bando *et al.* (30) observed that the Rh–Rh bond may be disrupted upon CO adsorption on Rh-containing zeolites. The same was found for Ru-based catalysts (44). Hence, in addition to the dispersion of the Rh particles, some surface carbonyls may be formed. However, it cannot be excluded that some Rh–O species are still present under reaction conditions.

Whereas the mass spectrometric analysis results (Fig. 4) show differences in selectivity dependent on the residence time (the maximum of the water formation is shifted to lower temperatures at higher residence times), also observed in other studies (9, 21, 22, 24), no significant structural differences were found when using different residence times (Fig. 6(2), curves a and b). Thus, the bulk structure of the clusters, as determined by *in situ* EXAFS, seems to be identical. Though most of the Rh atoms are on the surface, this might nevertheless be due to the fact that EXAFS monitors all Rh atoms on average. Hence, different surface

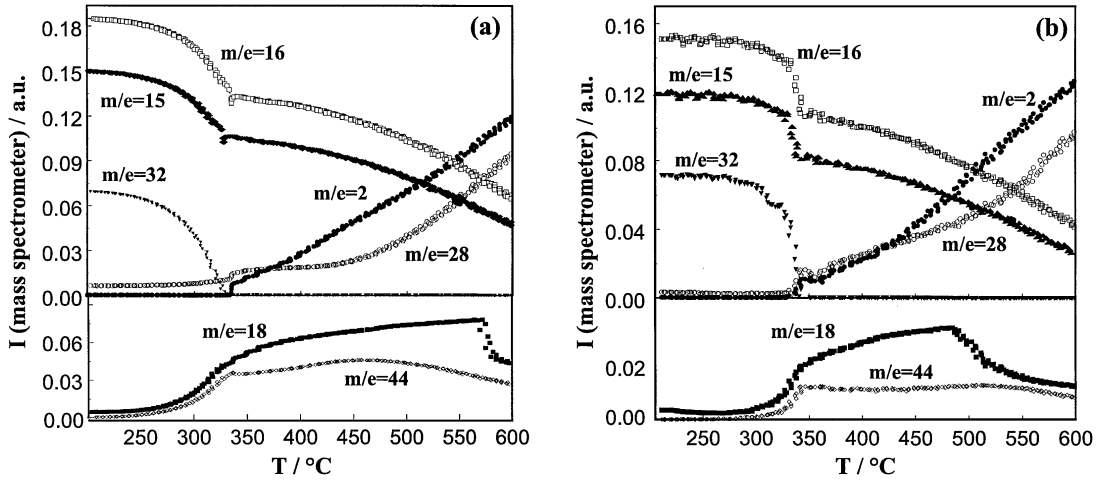

FIG. 4. Traces of different MS signals in the reaction mixture CH_4/O_2 with flow of (a) 1 ml/min and (b) 12 ml/min (step C) with signals for the educts CH_4 ($m/e = 15$, 16), O_2 ($m/e = 32$), the products CO ($m/e = 28$), H_2 ($m/e = 2$), and the by-products H_2O ($m/e = 18$), and CO_2 ($m/e = 44$).

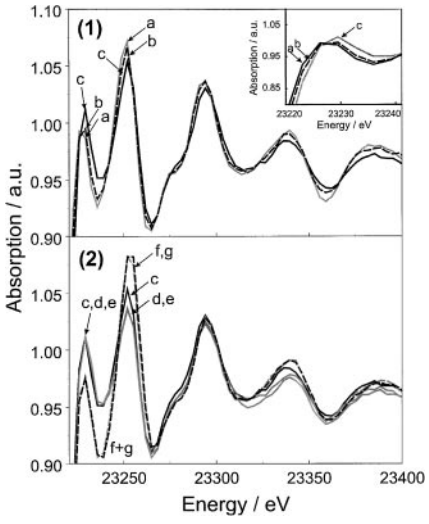

FIG. 5. Selected *in situ* QEXAFS data at the Rh K-edge during heating in CH_4/O_2 reaction mixture (step C) at (a) 25°C, (b) 120°C, (c) 250°C, (d) 300°C, (e) 320°C, (f) 335°C, and (g) 360°C (flow 1 ml/min).

structures and/or surface temperatures may be responsible for the different reactivities of the clusters. Different flow velocities may also influence the heat and mass transport conditions. In DRIFTS studies differences in the intensity and the positioning of the CO stretching bands have been found (22), especially when the samples only contained very low Rh concentrations (0.1 wt%).

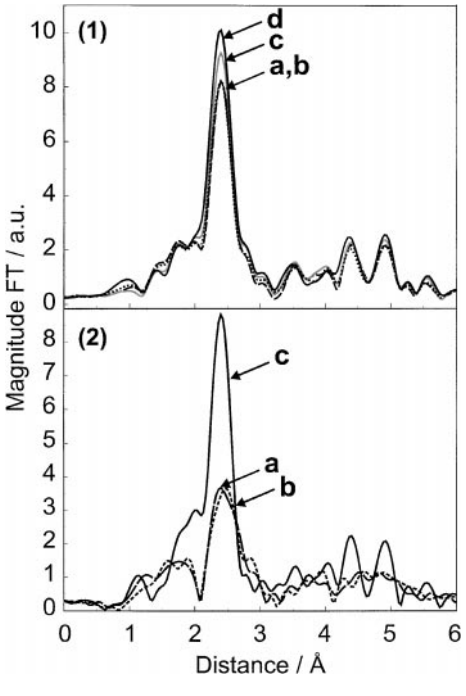

FIG. 6. Comparison of Fourier-transformed EXAFS spectra of the Rh K-edge: (1) cooled to room temperature in the corresponding reaction mixture after (a) treatment in CH_4/O_2 (12 ml/min, step C), (b) treatment in CH_4/O_2 (1 ml/min, step C), (c) treatment in H_2 (step B), and (d) Rh foil. (2) during (a) treatment in CH_4/O_2 (600°C, 12 ml/min, step C), (b) treatment in CH_4/O_2 (1 ml/min, 600°C, step C), (c) during treatment in H_2 at 500°C (step B).

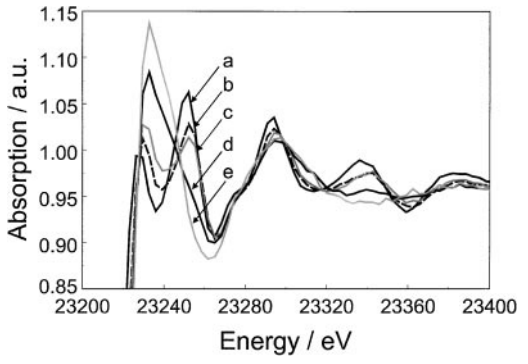

FIG. 7. *In situ* oxidation of Rh/Al_2O_3 (after step A) in 2% O_2 in He between RT and 500°C monitored by QEXAFS at (a) 80°C, (b) 240°C, (c) 300°C, (d) 410°C, and (e) 470°C.

3.5. Step D (Heating of the Catalyst in O_2)

Treatment of the Rh catalyst in an oxidising atmosphere was performed after step A (treatment in He), and Figure 7 depicts the *in situ* XAFS results. Interestingly, the change of the catalyst structure seems to proceed slowly in the temperature interval 250–450°C. As indicated by the increase of the whiteline (Figure 7) and the increase of intensity of peaks in the Fourier-transformed spectra around 1.5 Å (cf. Fig. 8), the catalyst is gradually oxidised. The

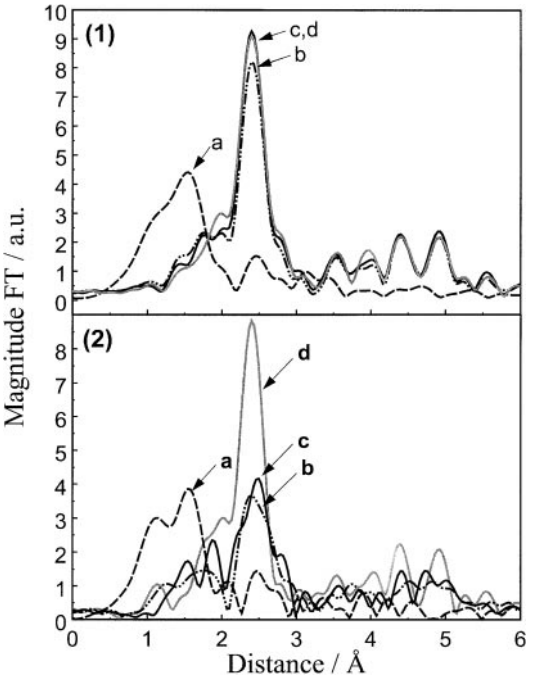

FIG. 8. Fourier transforms of k^1-weighted EXAFS oscillations at the Rh edge, at room temperature (1) and at 500/600°C (2): (a) after O_2 treatment (step D), (b) after CH_4 treatment (step E), (c) after CH_4/O_2 treatment (step C), and (d) after H_2/N_2 treatment (step B).

room-temperature data of the Fourier-transformed spectrum are plotted in Fig. 8(1) and comparison to Fig. 1 reveals that the catalyst is fully oxidised to Rh_2O_3 (see also the analysis listed in Table 4). Also, in DRIFTS studies, the oxidation of Rh was found at relatively low temperatures (22, 37), already starting at 100°C. Up to 300°C the oxidation of Rh in this step D is very similar to the structural changes in the CPO reaction mixture (step C). Hence, both the gradual oxidation of the catalyst according to EXAFS and the earlier oxidation of the catalysts observed in DRIFTS evidence that the catalyst in step C is oxidized upon heating in CH_4/O_2, especially on the external surface of the Rh clusters probably due to the oxygen present in the reaction mixture. The CPO reaction in step C first starts above 300°C when the concentration of oxygen is low in the outlet gas. Hence, this supports the hypothesis that metallic-like or carbonylic Rh species are involved in the CPO reaction.

3.6. Step E (Heating of the Oxidized Catalyst in CH_4)

In the last step, the oxidized catalyst (step D) was exposed to methane. In the mass spectrometer some water evolution was detected around 250°C. No reaction was detected at room temperature, in contrast to observations with DRIFTS (21, 22, 37). Above 250°C also H_2 evolution was detected. The QEXAFS data revealed that the catalyst is quickly reduced around 250°C. The Fourier-transformed EXAFS data of the catalyst after reduction are plotted in Figs. 8(1) (room-temperature data) and 8(2) (500°C data). Comparison of the high-temperature data of the catalysts under reaction conditions (step C versus step E) reveals that they are similar but not identical. This indicates that some carbonyl species could be present on the surface after these steps as proposed by the DRIFTS studies and that CO and H_2 can be produced by consumption of O_2 and CH_4 in separate steps (22).

4. CONCLUSIONS

In this study, the structure of Rh-carbonyl clusters has been monitored by *in situ* XAFS combined with on-line mass spectrometry during different reaction steps. XAFS gives information on the particle size, the oxidation state, and the bulk structure of the particles, while on-line product analysis directly uncovers the catalysis. The capillary setup is ideal for studying reactions at relatively short residence times (down to 0.05 s). This has given additional and complementary insight into the previously performed DRIFTS studies (21, 22, 37, 45). A schematic representation of the structural changes during the different steps is shown in Fig. 9.

Both XAFS and DRIFTS showed the decomposition of the $Rh_4(CO)_{12}$ precursor upon heating in He (step A) and further reduction in hydrogen (step B). However, the higher Rh loading used in this study also led to some structural differences. Whereas it was concluded from DRIFTS that $Rh^I(CO)_2$ forms on the surface (0.1 wt% Rh loading), we conclude from EXAFS that the Rh_4 tetrahedron as a structural unit is mainly preserved during anchoring of the precursor, probably due to the significantly higher loading (5 wt% Rh). But in both cases aggregative decarbonylation reactions occur during decomposition. The higher loading of Rh in the present study is probably also the reason why large Rh particles with a coordination number of 11–12 form upon reduction in hydrogen. These particles are found to be ~60Å according to XRD. Under reaction conditions (step C), we observe reversibly a series of structural transformations, including re-dispersion of the Rh particles. Upon heating the catalyst in the CH_4/O_2 reaction mixture, Rh is first oxidized at lower temperatures, which is very similar to the behaviour of the catalyst in step D (up to 300°C), where the catalyst is oxidized in oxygen. When the CPO reaction ignites, the catalyst abruptly changes its structure and is reduced. Moreover, a re-dispersion of the Rh particles occurs. During quenching to room temperature, the metallic character is preserved, but aggregation to larger particles is observed. Whereas the mass spectrometric analysis results show differences in selectivity dependent on the residence time, no significant structural differences are found by EXAFS.

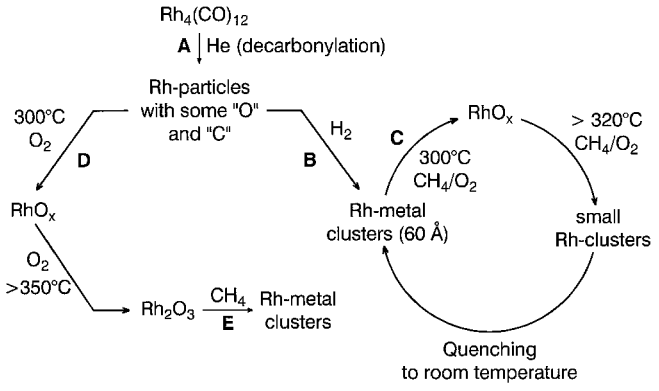

FIG. 9. Schematic representation of the structural changes during steps A–E (for more details, see text).

ACKNOWLEDGMENTS

The authors thank HASYLAB for offering beam time at beamline X1. We are grateful to K. Aasberg-Petersen and A. M. Molenbroek for helpful discussions, A. Kjersgaard and G. Steffensen for the help throughout the EXAFS measurements in Hamburg, and R. Christensen for *in situ* XRD measurements. Financial support from DANSYNC is gratefully acknowledged.

REFERENCES

1. Rostrup-Nielsen, J. R., *Catal. Today* **18**, 305 (1993).

2. Rostrup-Nielsen, J. R., "Catalysis Science and Technology" (J. R. Anderson and M. Boudart, Eds.), Vol. 5, p. 1. Springer Verlag, New York, 1984.
3. Christensen, T. S., and Primdahl, I. I., *Hydrocarbon Pros. Int. Ed.* **73**, 39 (1994).
4. Dybkjær, I., Presented at the 1996 Middle East Refining & Petrochemicals Conference and Exhibition, Bahrain, June 10–12, 1996.
5. Prettre, M., Eichner, C., and Perrin, M., *Trans. Faraday Soc.* **43**, 355 (1946).
6. Gavalas, G. R., Phichitcul, C., and Voeks, G. E., *J. Catal.* **88**, 54 (1984).
7. Dissanayake, D., Rosink, M. P., Kharas, K. C. C., and Lunsford, J. H., *J. Catal.* **132**, 117 (1992).
8. Foulds, G. A., and Lapzewicz, J. A., "Catalysis" (J. J. Spivey and S. K. Arganal, Eds.), Vol. 11, p. 412. The Royal Society of Chemistry, Cambridge, 1994.
9. Ashcroft, A. T., Cheetham, A. K., Green, M. L. H., and Vernon, P. D. F., *Nature* **352**, (1991).
10. Lapszewicz, J. A., and Jiang, X.-Z., *Prepr. Am. Chem. Soc. Div. Pet. Chem.*, **38**, 815 (1993).
11. Matsumara Y., and Moffat, J. B., *Catal. Lett.* **24**, 59 (1994).
12. Choudary, V. R., Mamman, A. S., and Sansare, S. D., *Angew. Chem. Int. Ed. Engl.* **31**, 1189 (1992).
13. Hickman, D. A., and Schmidt, L. D., *J. Catal.* **138**, 267 (1992).
14. Choudary, V. R., Rajput, A. M., and Prabhakar, B., *Catal. Lett.* **15**, 363 (1992).
15. Bharadwaj, S. S., and Schmidt, L. D., *Fuel Process. Technol.* **42**, 109 (1995).
16. Sissanake, D., Rosinek, M. P., and Lunsford, J. H., *J. Phys. Chem.* **97**, 3644 (1993).
17. Chang, Y. F., and Heinemann, H., *Catal. Lett.* **21**, 215 (1993).
18. Basini, L., and Aragno, A., *J. Chem. Soc. Faraday Trans.* **90**, 787 (1994).
19. Hickmann, D. A., and Schmidt, L. D., *React. Kinet. Catal.* **39**, 1164 (1993).
20. Basini, L., Aragno, A., and Vlaic, G., *Catal. Lett.* **39**, 49 (1996).
21. Basini, L., Guarinoni, A., and Aasberg-Petersen, K., *Stud. Surf. Sci. Catal.* **119**, 699 (1998).
22. Basini, L., Guarinoni, A., and Aragno, A., *J. Catal.* **190**, 284 (2000).
23. Alibrando, M., Hahm, H. S., and Wolf, E. E., *Catal. Lett.* **49**, 1 (1997).
24. Hofstadt, K. H., Hoebink, J. H. B. J., Holmen, A., and Martin, G. B., *Catal. Today* **40**, 157 (1998).
25. van't Blik, H. F., van Zon, J. B. A. D., Huizinga, T. Vis, J. C., Koningsberger, D. C., and Prins, R., *J. Phys. Chem.* **87**, 2264 (1983).
26. van't Blik, H. F. J., van Zon, J. B. A., Huiziga, T., J. C. Vis, Koningsberger, D. C., and Prins, R., *J. Am. Chem. Soc.* **107**, 3139 (1985).
27. Gloor, A. P., and Prins, R., *J. Phys. Chem.* **39**, 9867 (1994).
28. Cimini, F., and Prins, R., *J. Phys. Chem.* **101**, 5277(1997).
29. Cimini, F., and Prins, R., *J. Phys. Chem.* **101**, 5285 (1997).
30. Bando, K. K., Ichikuni, N., Soga, K., Kunimori, K., Arakawa, H., and Asakura, K., *J. Catal.* **194**, 91 (2000).
31. Weber, W. A., Zhao, A., and Gates, B. C., *J. Catal.* **182**, 13 (1999).
32. Medvedev, V. K., Suchorski, Y., Voss, C., de Bocarme, T. V., Bar, T., and Kruse, N., *Langmuir* **14**, 6151 (1998).
33. Voss, C., and Kruse, N., *Surf. Sci.* **409**, 252 (1998).
34. Clausen, B. S., Steffensen, G., Fabius, B., Villadsen, J., Feidenhans'l, R., and Topsøe, H., *J. Catal.* **132**, 524 (1991).
35. Clausen, B. S., Gråbæk, L., Steffensen, G., Hansen, P. L., and Topsøe, H., *Catal. Lett.* **20**, 23 (1993).
36. Grunwaldt, J.-D., Molenbroek, A. M., Topsøe, N.-Y., Topsøe, H., and Clausen, B. S., *J. Catal.* **194**, 452 (2000).
37. Basini, L., Marchionna, M., and Aragno, A., *J. Phys. Chem.* **96**, 9431 (1992).
38. Wei, C. H., *Inorg. Chem.* **8**, 2385 (1969).
39. Als-Nielsen, J., Grübel, G. and Clausen, B. S., *Nucl. Instrum. Methods Phys. Res. Sect. B* **97**, 522 (1995).
40. Clausen, B. S., *Catal. Today* **39**, 293 (1998).
41. Iwasawa, Y., "X-ray absorption fine structure for catalysts and surfaces" Vol. 2, World Scientific, Singapore, 1996.
42. Clausen, B. S., and Nørskov, J. K., *Top. Catal.* **10**, 221 (2000).
43. Asakura, K., Iwasawa, Y., and Kuroda, H., *J. Chem. Soc. Faraday Trans. 1* **84**, 1329 (1988).
44. Mizushima, T., Tohij, K., Udagawa, Y., and Ueno, A., *J. Am. Chem. Soc.* **112**, 7887 (1990).
45. Basini, L., and Sanfilippo, D., *J. Catal.* **157**, 162 (1995).